





Cite this: *J. Mater. Chem. B*, 2022, 10, 2038

## Design and characterization of fibroblast activation protein targeted pan-cancer imaging agent for fluorescence-guided surgery of solid tumors†

Ramesh Mukkamala,  Spencer D. Lindeman,  Kate A. Kragness, Imrul Shahriar, Madduri Srinivasarao and Philip S. Low\*

Tumor-targeted fluorescent dyes have been shown to significantly improve a surgeon's ability to locate and resect occult malignant lesions, thereby enhancing a patient's chances of long term survival. Although several tumor-targeted fluorescent dyes have been developed for imaging specific subsets of human cancers, no tumor-targeted dye has been designed that can image all cancer types. Based on observations that fibroblast activation protein (FAP) is upregulated on cancer-associated fibroblasts (CAFs) that infiltrate essentially all solid tumors, we have undertaken to develop a FAP-targeted fluorescent dye that can image CAFs without accumulating in healthy cells or fibroblasts. We report here that FTL-S-S0456, a novel FAP-targeted near infrared dye that binds FAP with high affinity (~12 nM) and specificity (>5000-fold over PREP and DPP-IV), concentrates in all seven solid tumor types examined, yielding fluorescence images with high tumor to background ratios that persist for several days. We conclude that FTL-S-S0456 constitutes an excellent ligand-targeted near infrared dye that enables intra-operative imaging of most if not all solid tumors.

Received 1st December 2021,  
Accepted 20th February 2022

DOI: 10.1039/d1tb02651h

rsc.li/materials-b

### Introduction

According to the American Cancer Society, 1 898 160 new cancer cases and 608 570 cancer deaths are projected to occur in the United States in 2021,<sup>1</sup> and this incidence is anticipated to increase as the population ages.<sup>1</sup> Although surgical resection of all malignant lesions constitutes the only reliable cure for cancer, complete responses are still not always achieved due to failure to detect all neoplastic tissues, resulting in local recurrence and sometimes death.<sup>2–4</sup> Indeed, up to 40% of breast cancers,<sup>5</sup> 50% of ovarian cancers,<sup>6</sup> 40% of non-small cell lung cancers (NSCLC)<sup>7</sup> and 34% of small cell lung cancers<sup>8</sup> recur in the original tumor bed, suggesting that the initial surgery was not successful in resecting all diseased tissue. While different imaging modalities such as ultrasonography, magnetic resonance imaging (MRI), computed tomography (CT), positron emission tomography (PET) and single photon emission computed tomography (SPECT) have been explored for enhanced intra-operative detection of cancer, none of these

methods has achieved widespread adoption, because either (i) image resolution has been inadequate for detection of small malignant lesions, (ii) image reconstruction has been too slow for intra-operative decision-making, (iii) imaging hardware has been too bulky for interrogation of confined body cavities, or (iv) radiation exposure associated with tumor imaging has been considered harmful to medical staff. Thus, the most successful intra-operative imaging modalities tested to date have involved optical detection of malignant lesions using tumor-targeted fluorescent dyes.<sup>9–12</sup>

The first use of a ligand-targeted fluorescent dye for localization and resection of a human cancer was performed by Gooitzen van Dam and colleagues<sup>13</sup> who were able to identify and resect five times more malignant lesions from ovarian cancer patients with the aid of a folate receptor-targeted fluorescein dye than using traditional methods of visual inspection and palpation. Encouraged by this success, additional ligand-targeted fluorescent dyes<sup>14–21</sup> and tumor-activated fluorescent probes<sup>22–25</sup> were gradually developed to expand the types of tumors that could be imaged. However, while most fluorescent probes developed to date display good tumor to background ratios (TBR) in a subset of tumors, no current dye yields quality images in the majority of tumors, thereby requiring development of a plethora of imaging agents for detection of all solid tumors.

Department of Chemistry and Institute for Drug Discovery, Purdue University, West Lafayette, Indiana 47907, USA. E-mail: plow@purdue.edu; Fax: +765496-2677; Tel: +765494-5283

† Electronic supplementary information (ESI) available. See DOI: 10.1039/d1tb02651h

In an effort to identify a pan-tumor marker for use in imaging all solid tumors, several laboratories have focused on the observations that cancer associated fibroblasts (CAFs) infiltrate almost all solid tumors<sup>26,27</sup> and that these CAFs frequently constitute the major stromal cell type in the malignant masses. Based on the additional facts that (i) CAFs can be distinguished from fibroblasts in healthy tissues by their expression of fibroblast activation protein alpha (FAP), (ii) more than 90% of epithelial cancers overexpress FAP,<sup>26,28,29</sup> and (iii) the level of FAP expression correlates negatively with patient survival,<sup>29–32</sup> several laboratories have undertaken to develop FAP-targeted imaging agents for detection, localization, and quantitation of solid tumors.<sup>33,34</sup> Indeed, Haberkorn and colleagues<sup>35</sup> have designed a FAP-targeted PET agent using a targeting ligand designed by Jansen *et al.*<sup>36,37</sup> to image 28 different human cancer types with excellent tumor to background ratios.<sup>27</sup> Other labs have exploited the dipeptidyl peptidase activity of FAP to create peptidase-activated dyes for fluorescence imaging of tumors,<sup>38,39</sup> and still others have used anti-FAP antibodies<sup>40–42</sup> to target fluorescent probes specifically to CAF-enriched cancer masses.<sup>41</sup> Most recently, both Pomper's<sup>43,44</sup> and our labs<sup>45</sup> have explored the use of low molecular weight FAP-targeting ligands to concentrate near infrared fluorescent dyes specifically in solid tumors. However, while most FAP-targeted NIR dyes display excellent tumor uptake, many also exhibit unwanted accumulation in healthy tissues (*e.g.*, stomach, liver, intestinal tract) and still others suffer from short tumor retention times that prohibit their uses for longer lasting surgeries.<sup>43,45</sup> To address these deficiencies, we undertook to design, synthesize, and test a FAP-targeted near infrared fluorescent dye that would not only bind FAP with high affinity and specificity, but also internalize into CAFs and remain there for prolonged periods of time. We demonstrate here that a novel FAP inhibitor can be designed with Schrödinger software and exploited to deliver a near infrared fluorescent dye with high specificity and affinity to at least seven different tumor types, yielding high contrast, long lasting

images of malignant lesions with little or no retention in healthy tissues. The data collectively suggest that the novel FAP-targeted fluorescent dye (FTL-S-S0456) may constitute a pan-cancer NIR fluorescence imaging agent that can be exploited for fluorescence guided surgery of most solid tumors.<sup>46</sup>

## Results and discussion

### Design and synthesis of a novel FAP-targeting ligand and its fluorescent conjugates

The scaffold of our FAP-targeting ligand was designed based on the structure of a FAP inhibitor **1** previously reported by Tsai *et al.*<sup>47</sup> Use of Schrödinger software to dock **1** into the binding pocket of **1** for FAP (Fig. 1a) revealed that attachment of carefully chosen substituents could enhance both the binding affinity and specificity of **1** for FAP (Fig. 1b and Fig. S12a–c, ESI†), while concurrently creating a functional group for conjugation to a fluorescent dye (*i.e.*, phenoxy-S0456). Because this molecular modeling also revealed that the 2,3-dihydro isoindole ring of **1** should remain solvent exposed after binding to FAP (Fig. 1a), we elected to link the near infrared fluorescent dye (S0456) to the 4th position of the 2,3-dihydro isoindole ring *via* a phenyltriazole-derivatized PEG<sub>4</sub>-amine to generate precursor **2**. Precursor **2** was then synthesized as shown in Scheme S1 (see ESI†) and then reacted with 4-hydroxyphenyl propionic acid to yield precursor (**3**) followed by conjugation with the cyanine dye (Cl-S0456) to provide the final FAP-targeted NIR dye **4** (Fig. 2 and see ESI† Scheme S2).

### Evaluation of the affinity and specificity of FAP-targeted fluorescent dyes for cancer associated fibroblasts

Because most previous FAP-targeted imaging agents have been compromised by unwanted uptake in healthy tissues and/or inadequate retention times in malignant tissues,<sup>43,45,48</sup> it was important to examine both the FAP specificity and tumor retention times of FAP-targeted conjugates **3** and **4** before proceeding with studies in live animals. To evaluate the specificity

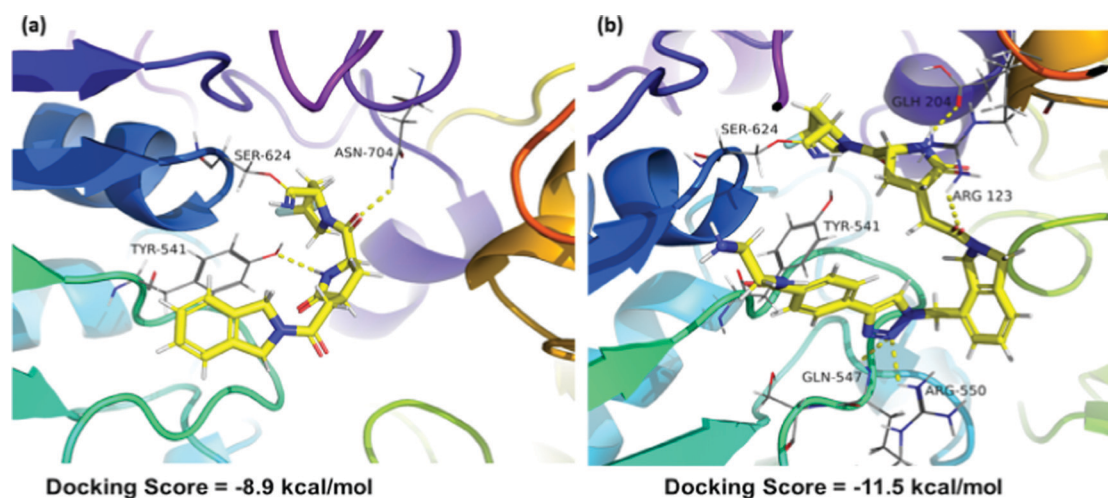


Fig. 1 Modelled binding mode of (a) inhibitor (**1**) and (b) FTL-S-Ligand docked with human Fibroblast Activation Protein alpha (PDB ID: 1Z68).

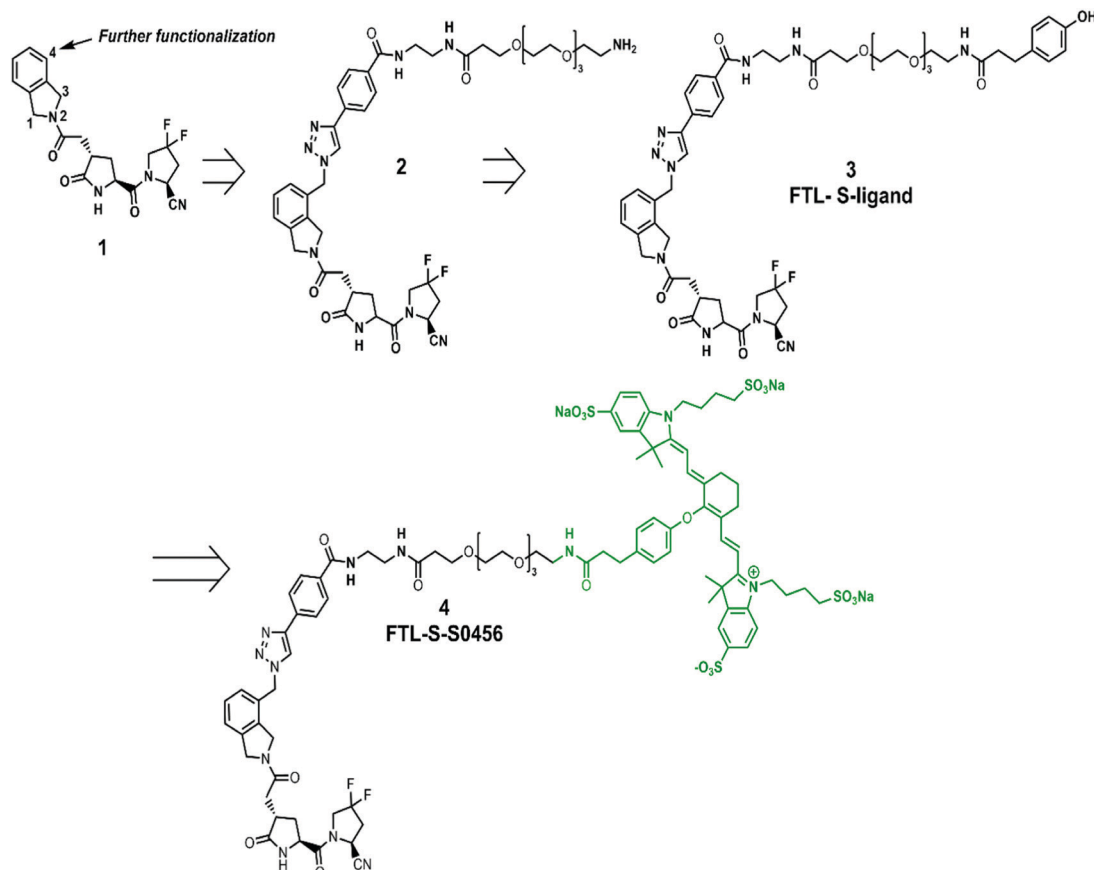


Fig. 2 Chemical structures of fibroblast activation protein (FAP) inhibitor (**1**), FAP targeting ligand with linker (FTL-PEG4-NH<sub>2</sub>) (**2**), the conjugate of **2** with 4-hydroxyphenyl propionic acid (**3**) and the conjugate of **3** with Cl-S0456 (**4**).

of **3** and **4** for FAP relative to its ubiquitous homologs, dipeptidyl peptidase-IV (DPP-IV) and prolyl oligopeptidase (PREP), the ability of **3** and **4** to inhibit FAP, DPP-IV and PREP were compared. As shown in (Fig. 3), ligands **3** and **4** were able to inhibit purified FAP with an IC<sub>50</sub> of 2.1 nM and 2.3 nM respectively (Table 1), whereas their inhibition of both PREP and DPP-IV were >10 μM, *i.e.*, suggesting that any unwanted binding to healthy tissues expressing PREP or DPP-IV should be minimal. It is also worth noting that both FTL-S-

ligand (**3**) and FTL-S-S0456 (**4**) exhibited tenfold better inhibition of FAP than its predecessor **1** (IC<sub>50</sub> = 2.1 *versus* 22 nM),<sup>47</sup> as predicted by the docking scores in Fig. 1.

#### Analysis of binding and internalization of FAP-dye conjugate **4** *in vitro*

With the affinity and specificity of **3** and **4** for FAP established, it became important to determine whether **4** could deliver an

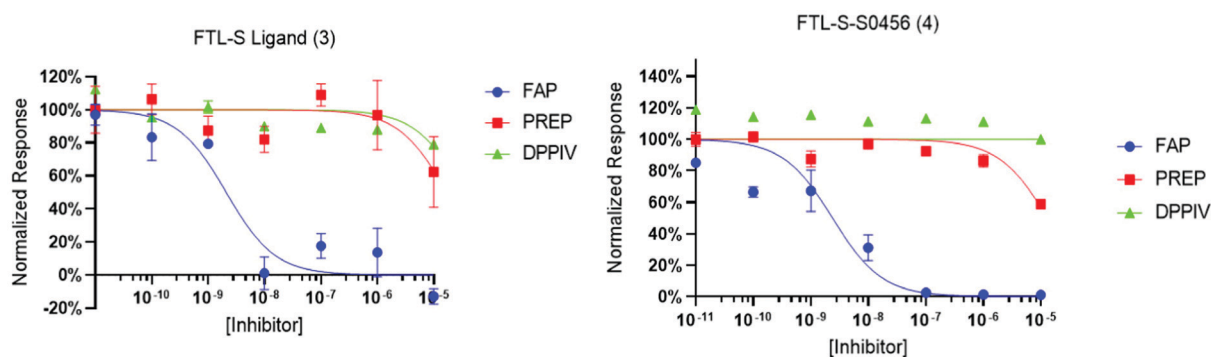


Fig. 3 Analysis of the ability of FTL-S-Ligand (**3**) and FTL-S-S0456 (**4**) to inhibit the closely related dipeptidyl peptidases FAP, PREP and DPP-IV. FAP, PREP and DPP-IV were incubated with **3** and **4** for 10 minutes at room temperature prior to addition of fluorogenic substrate. After allowing the reaction to proceed for 30 min at 37 °C, the reaction was terminated and the change in fluorescence was quantitated as a measure of catalytic activity. All assays were performed in triplicate, with SEM bars shown.

**Table 1** Inhibition of FAP, PREP and DPP-IV by compound **3** and **4**

Compound	IC <sub>50</sub> (μM)			<sup>a</sup> FAP Selectivity
	FAP	PREP	DPP-IV	
<b>1</b> <sup>b</sup>	0.022	n.d	>100	n.d
<b>3</b>	0.0021	17.0	>100	8095
<b>4</b>	0.0023	13.6	>100	5652

<sup>a</sup> FAP selectivity is equal to IC<sub>50</sub>(PREP)/IC<sub>50</sub>(FAP). <sup>b</sup> IC<sub>50</sub> of known inhibitors (**1**) according to reference.<sup>47</sup> n.d: not determined.

attached fluorescent dye into FAP-expressing cells. For this purpose, **4** was incubated with human FAP-transfected HT1080 cells (HT1080-FAP) (see methods for transduction of HT1080 with hFAP & Fig. S1, ESI†) and examined for uptake of fluorescence in the presence and absence of excess unlabeled ligand **3**. As shown in the confocal images of (Fig. 4A), FTL-S-S0456 (**4**) was able to label HT1080-FAP cells intensely in the absence of competing **3** (panels ii and iii), but not in the presence of excess **3** (panels v and vi), *i.e.*, demonstrating that binding of FTL-S-S0456 (**4**) to HT1080-FAP cells was FAP-mediated. More detailed examination of the confocal images (panel ii and iii) further revealed that a significant fraction of the bound fluorescence resided in punctate compartments inside the cells, demonstrating that the fluorescent conjugate can indeed internalize into intracellular endosomes. Importantly, this internalization could be confirmed by examining the colocalization of FTL-S-S0456 (**4**) with the late endosomal marker (Rb5a-GFP). As shown in confocal images (panel vii to

ix), FTL-S-S0456 (**4**) and Rb5a-GFP clearly localize to the same endosomal compartments. More quantitative analysis of the binding of **4** to HT1080-FAP cells is shown in the binding isotherms of (Fig. 4B), where FTL-S-S0456 (**4**) is found to bind whole cells with a  $K_d = 12.0$  nM. That this binding is also FAP-mediated is again established by both the absence of binding of the targeted dyes to HT1080 cells lacking FAP (red symbols) as well as the suppression of binding to HT1080-FAP cells seen in the presence of excess unlabeled **3** (green symbols).

### In Vivo imaging and biodistribution

Whereas previous studies of FAP-targeted imaging agents have generally employed cancer cells that were transfected with FAP in order to create tumors with high FAP contents,<sup>35,49,50</sup> to determine whether FTL-S-S0456 might be capable of imaging a more physiologically relevant tumor, we implanted FAP negative KB cell<sup>45</sup> tumors into athymic nu/nu mice to generate solid tumors whose sole source of FAP would be infiltrating cancer associated fibroblasts (CAFs). After allowing the tumors to grow to ~400 mm<sup>3</sup>, the mice were injected intravenously with increasing concentrations of FTL-S-S0456 and imaged two hours later. As shown in (Fig. S2, ESI†), minimal tumor fluorescence was seen in mice treated with only 0.3 nmol FTL-S-S0456 per mouse, but strong tumor fluorescence was visible at 1.0 nmol FTL-S-S0456/mouse and all higher concentrations. Because healthy tissues (except the kidneys, where the conjugate undergoes excretion) became fluorescent only at FTL-S-S0456 concentrations ≥10 nmol per mouse, we concluded

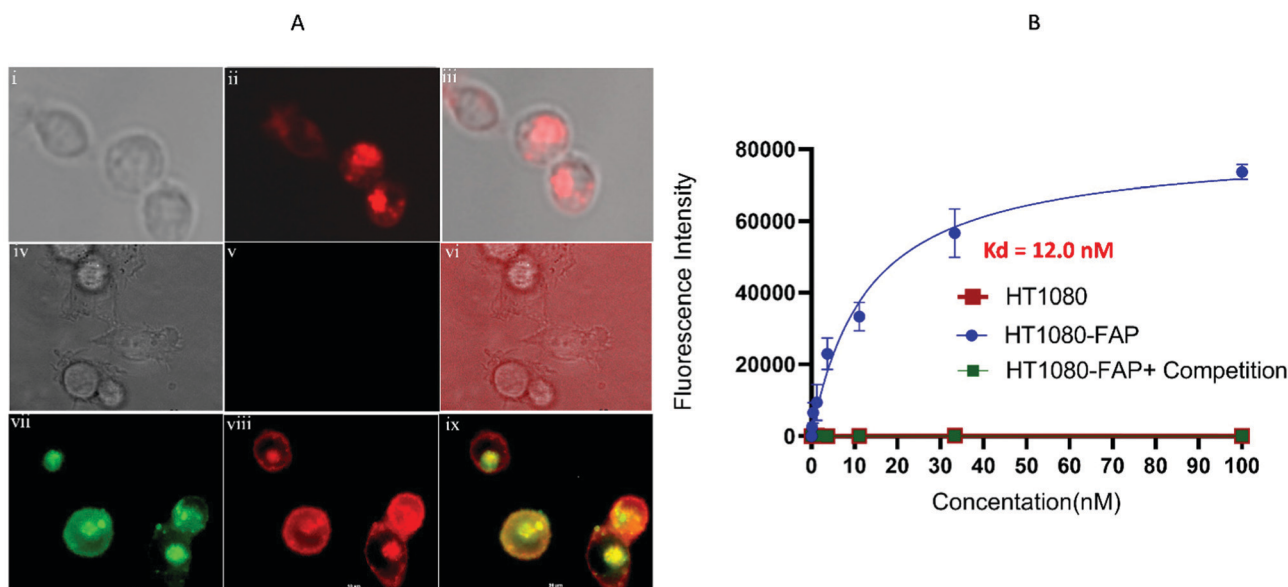


**Fig. 4** Analysis of binding and internalization of FTL-S-S0456 conjugate (**4**) by HT1080-FAP cells. (A) Images of HT1080-FAP cells taken 1 hour after addition of FTL-S-S0456. HT1080-FAP cells were incubated with 25 nM FTL-S-S0456 (**4**) and examined by wide-field Nikon confocal microscopy. Bright field images (panels i and iv) and fluorescence images (panels ii and v) are merged in (panels iii and vi) in the absence and presence of excess unlabeled ligand **3**, respectively. HT1080-FAP cells that were transfected with the endosomal marker (Rb5a-GFP) using a CellLight BacMam 2.0 kit (Invitrogen) were also incubated with FTL-S-S0456 and imaged 1 hour later. Rb5a-GFP staining is shown in green (panel vii), whereas FTL-S-S0456 is shown in red (panel viii). Colocalization of FTL-S-S0456 with Rb5a-GFP is shown in yellow (panel ix). Scale bar = 10 μm (B) The binding affinity and specificity of increasing concentrations of FTL-S-S0456 was further established in live cells by measuring FTL-S-S0456 fluorescence following its incubation with either HT1080-FAP cells (green and blue symbols) or HT1080 cells (red symbols) for 1 h at 4 °C in the presence (green symbols) or absence (blue and red symbols) of 100-fold excess unlabeled ligand **3**.



that good tumor to background ratios could be achieved in mice bearing KB tumors at all FTL-S-S0456 concentrations between 1 and 10 nmol per mouse, with perhaps the optimal dose centering at  $\sim 5$  nmol per mouse.

Next, because CAFs are reported to accumulate in virtually all solid tumors,<sup>26</sup> the question arose whether a diversity of tumor types might similarly recruit sufficient CAFs to enable FTL-S-S0456 imaging. To address this question, we selected seven different cancer cell lines deriving from seven distinct

tumor types, namely human triple negative breast cancer (MDA-MB-231), human colorectal cancer (HT29), human glioblastoma (U87MG), human head and neck cancer (FADu), human pancreatic cancer (PANC-1), murine breast cancer (4T1) and human nasopharyngeal cancer (KB) and implanted the cells in appropriate recipient mice. After allowing tumors to grow to  $\sim 400$  mm<sup>3</sup>, mice were injected with 5 nmol FTL-S-S0456 and again imaged 2 hours later. As shown in (Fig. 5, panels A and C), FTL-S-S0456 displayed good uptake in all seven

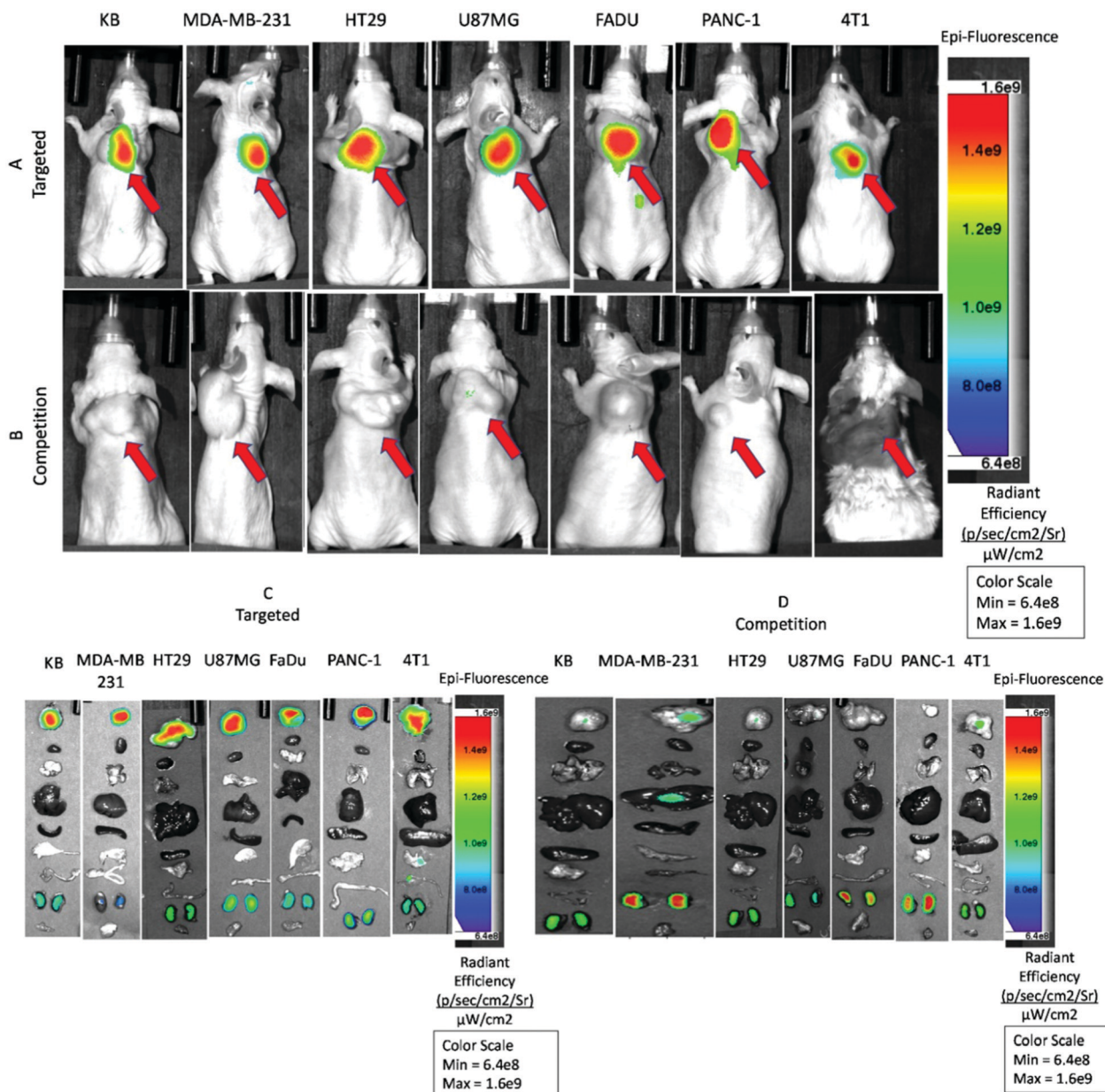


**Fig. 5** Examination of the ability of FTL-S-S0456 to image diverse tumor types. Mice were implanted with KB, MDA-MB-231, HT29, U87MG, FaDu, PANC-1 or 4T1 tumor cells and tumors were allowed to grow to  $\sim 400$  mm<sup>3</sup> prior to intravenous injection of 5 nmol FTL-S-S0456 (**4**) either in the absence (A and C) or presence (B and D) of excess FAP-ligand **3**. Two hours post injection mice were euthanized and imaged using an AMI imager. U87MG cells were the only tumor cells that naturally express FAP. Mice from panels (A and B) were dissected and the biodistribution of FTL-S-S0456 is shown in the fluorescence images of panels (C and D). The tissues examined from top to bottom are tumor, heart, lungs, liver, spleen, stomach, small intestine, kidneys, and muscle. All the images throughout the study were acquired using the same imaging parameters across the tumor type and images in targeted and competition groups were adjusted to same scale bar within each tumor type. Red arrow indicates tumor and  $n = 5$  mice per group.

tumor types, with excellent tumor to background ratios ranging from an average of 8:1(tumor:heart), 8:1(tumor:lung), 5:1(tumor:liver), 7:1(tumor:spleen), 11:1(tumor:stomach), 6:1(tumor:intestine), 2:1(tumor:kidney) to 26:1(tumor:muscle). That this tumor uptake was FAP-mediated could be established by comparing the tumor accumulation of FTL-S-S0456 in mice simultaneously injected with either saline or a competing concentration (100 $\times$ ) of unlabeled FAP ligand **3**. Thus, as seen in panel B and D, tumor retention was blocked by

excess **3**, while excretion through the kidneys was not. In fact, the only healthy tissue that showed significant S0456 fluorescence at this 2 hour time point was the kidneys, where FTL-S-S0456 was still undergoing excretion. Furthermore, because U87MG cells were the only cells to naturally express FAP,<sup>51,52</sup> these data suggest that sufficient CAFs must infiltrate the six other tumor types to enable high contrast FTL-S-S0456 imaging (see more detailed images in Fig. S3–S9, ESI<sup>†</sup>).

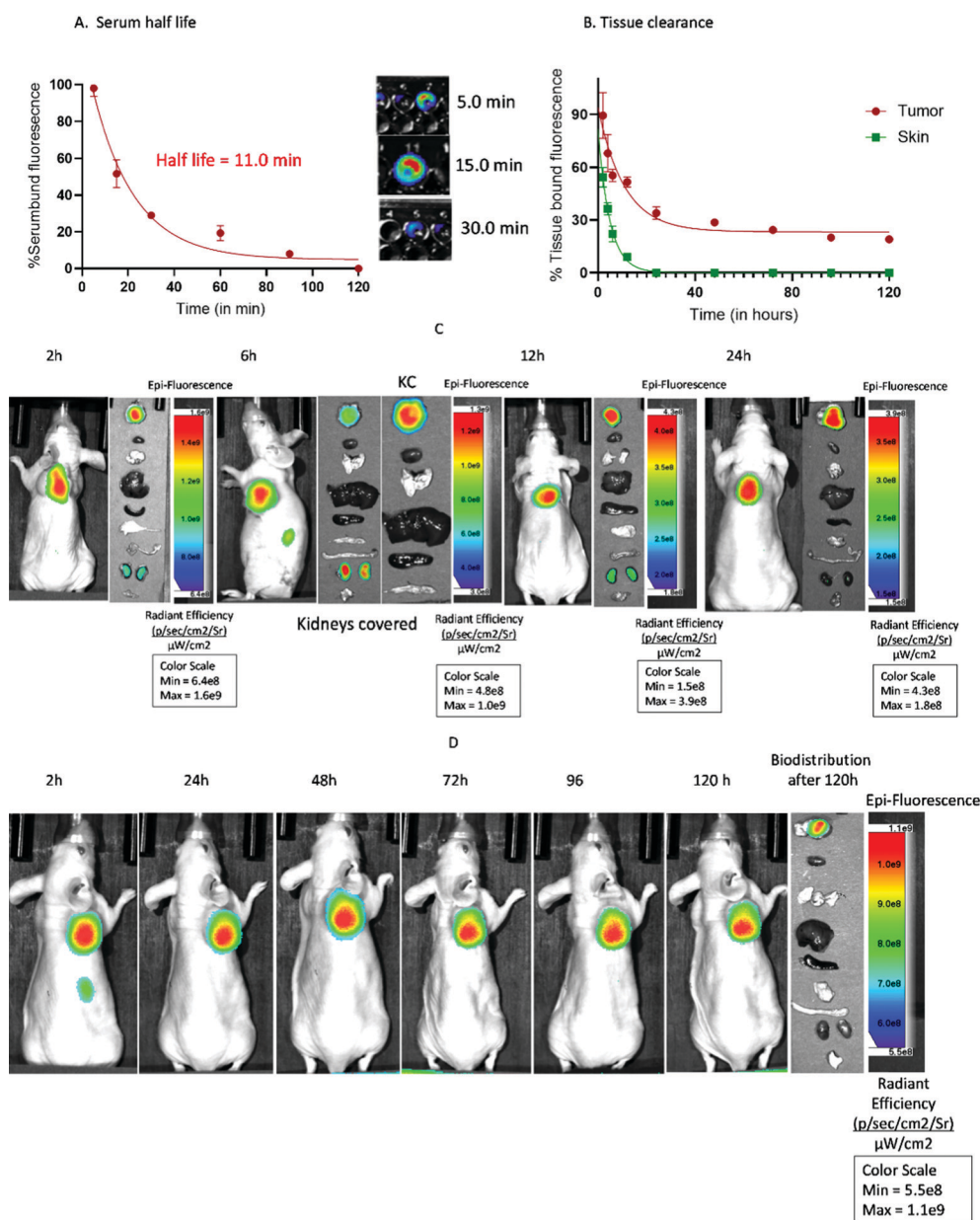


**Fig. 6** Evaluation of the PK profile of FTL-S-S0456 to KB cell tumors in athymic nu/nu mice. (A) Determination of the half-life of FTL-S-S0456 by time dependent serum bound fluorescence analysis. Healthy athymic nu/nu mice were intravenously injected with 10 nmol of FTL-S-S0456 and blood was collected at different time intervals and serum bound fluorescence was measured by using AMI imager. Error bar represents ( $n = 3$  mice per time point). (B) Determination of skin clearance of FTL-S-S0456 in the tumor bearing mice ( $n = 3$  mice per group) at different time points. (C) Whole body and biodistribution of FTL-S-S0456 in the indicated tissues of the KB tumor bearing mice ( $n = 3$  mice per group) sacrificed 2 hours after FTL-S-S0456 injection. The organs from top to bottom are tumor, heart, lung, liver, spleen stomach, small intestine, kidneys, and muscle. (D) Analysis of the time course of uptake of FTL-S-S0456 in the aforementioned mice ( $n = 3$  mice per group) implanted with FAP-negative KB cells.

### Evaluation of the PK properties of FTL-S0456

Finally, because anti-FAP antibodies require many hours to clear from healthy tissues,<sup>41,42</sup> whereas the low molecular weight FAP-targeted dyes examined to date have remained only transiently in the tumor masses,<sup>43,45,53</sup> it was important to determine the rate of clearance of FTL-S-S0456 from the blood and healthy tissues, and the duration of FTL-S-S0456 retention in tumor masses. To quantitate the half-life of FTL-S-S0456 in the blood, FTL-S-S0456 was injected intravenously into mice (10 nmol per mouse) and blood was collected at different time intervals (5–180 min) post-injection. As shown in (Fig. 6A), FTL-S-S0456 fluorescence was cleared from the blood with a half-life of ~11 minutes, suggesting that the imaging agent departs sufficiently rapidly from FAP negative compartments to allow tumor visualization within an hour post-injection. From our perspective, this rapid clearance is desirable, since it would allow a surgeon to perform surgery shortly after dye injection. As a surrogate for healthy tissues, we also quantitated clearance of FTL-S-S0456 from the skin, where its fluorescence would not be significantly absorbed by overlying tissues. As shown in (Fig. 6B), FTL-S-S0456 exited the skin with a half-time of ~2 hours and was completely cleared by 16 hours post injection. Indeed, even the kidneys (*i.e.*, the site of excretion) were cleared of FTL-S-S0456 between 12 and 24 hours post-injection (Fig. 6C).

Finally, to determine how long FTL-S-S0456 might remain in a tumor mass before its metabolism or excretion, mice implanted with KB tumors were injected and imaged as above, only the imaging was performed over a 120 hour time span. As shown in (Fig. 6D), fluorescence remained bright in all tumors for the entire 120 hour duration of the study, suggesting its retention in KB tumors was sufficiently long for any normal surgery. Moreover, as shown in (Fig. S3, ESI<sup>†</sup>), retention of FTL-S-S0456 in MDA-MD-231 tumors (the only other tumor model examined in this retention study) was similarly prolonged. When considered in combination with the broad tumor specificity of FTL-S-S0456 and its rapid clearance from healthy tissues, these data argue that FTL-S-S0456 exhibits the most important properties of a pan-cancer targeted fluorescent dye for use in fluorescence guided surgeries. To the best of our knowledge, no other fluorescent contrast agent exhibits all of these desirable properties.

Cancer associated fibroblasts are recruited/induced by virtually all solid tumors, where they perform such tumor-supportive functions as secretion of immunosuppressive cytokines,<sup>54</sup> release of tumor growth and angiogenic factors,<sup>54</sup> deposition of extracellular matrix (ECM) proteins (that suppress T cell infiltration)<sup>55,56</sup> and facilitation of cancer cell invasion and metastasis.<sup>57</sup> Upon entry into tumor masses, fibroblasts become activated by cytokines such as TGF- $\beta$  and differentiate into myofibroblasts,<sup>58</sup> which in turn express fibroblast activation protein (FAP) that distinguishes them from normal fibroblasts in healthy tissues. By designing a ligand-drug conjugate that targets only FAP, an attached drug can be concentrated in cancer tissues with little or no accumulation in healthy tissues.

Indeed, a recent study comparing a FAP-targeted PET imaging agent with the classical <sup>18</sup>F-FDG-PET for solid tumor imaging reported a consistently better tumor to background ratio for the FAP-targeted agent, because the background in healthy tissues was invariably much lower than that seen with <sup>18</sup>F-FDG-PET.<sup>59–61</sup> More importantly, this low healthy tissue background is expected to be even more pronounced with FTL-S-S0456, since its specificity for FAP over its ubiquitous homolog, DPP-IV, is ~10 000-fold (Fig. 3). Furthermore, because CAFs are not mutating, loss of FAP from tumor tissues due to cancer mutagenesis should be limited, enabling FAP-mediated imaging of solid tumors even when the cancer cells are evolving rapidly.

With the exploration of a new FAP targeting ligand for drug delivery, it was important to confirm that the desirable properties of previous FAP ligands were not lost when the new scaffold was employed. Indeed, as noted above, while the ability of FTL-S-S0456 to image many tumor types was still maintained, specificity for FAP may have actually improved, and tumor retention was unequivocally enhanced. Thus, although previous FAP-targeted imaging agents have been observed to remain in malignant lesions only few hours, a substantial fraction of FTL-S-S0456 was retained in the tumors indefinitely. Whether this prolonged retention derives from the ability of FTL-S-S0456 to efficiently internalize into FAP-expressing cells cannot be deduced from the data, but it clearly distinguishes FTL-S-S0456 from previous FAP-targeted drug conjugates. And while such protracted accumulation in cancer tissues may provide only occasional benefit to intra-operative imaging, such prolonged tumor retention could constitute a significant advantage for FAP-targeted radiotherapies, since the more common radiotherapeutic nuclides used in radioligand therapies have radiation half-lives of many days (*e.g.* <sup>177</sup>Lu,  $t_{1/2}$  = 6.65 days and <sup>225</sup>Ac,  $t_{1/2}$  = 9.92 days) and prolonged retention in a tumor without concomitant irradiation of healthy tissues could constitute a primary parameter that determines therapeutic efficacy.

## Conclusion

In an effort to develop a tumor-targeted near infrared dye that would be capable of imaging most solid tumors, we designed a FAP-targeted fluorescent imaging agent that binds to cancer associated fibroblasts but not to quiescent fibroblasts or cells in healthy tissues. The resulting FAP-conjugated S0456 dye not only accumulates specifically in all solid tumor types tested, but also causes malignant lesions to fluoresce brightly for several days following intravenous administration. Since a recently FDA-approved folate-targeted S0456 conjugate has been shown to enable intra-operative visualization of otherwise undetectable lesions in 27% of ovarian cancer patients,<sup>62</sup> we conclude that the fluorophore (S0456) attached to FTL-S-S0456 is capable of revealing occult lesions when concentrated in such lesions by receptor-mediated uptake. We therefore propose that



FTL-S-S0456 warrants continued development as a potential pan-cancer fluorescent imaging agent.

## Author contributions

Ramesh Mukkamala: Design and performance of experiments, methodology development, data analysis and interpretation, drafting of manuscript and critical revision, Spencer Lindeman: Development of transfected FAP cells, performance of experiments and interpretation of data, Kate Kragness: conduction of experiments, Imrul Shahriar: Design and molecular docking studies, Madduri Srinivasarao: Reviewing the manuscript, Philip S. Low: Study conception and design, guidance of researchers, drafting and critical revision of manuscript.

## Conflicts of interest

PSL owns stock in On Target Laboratories Inc. which could choose to license this technology from Purdue University.

## Acknowledgements

This work was supported by endowed chair funds from Purdue University and a grant from On Target Laboratories Inc. Authors would like to thank the Purdue Imaging Facility and Maria Isabel Olivero Acosta, for assistance with data collection, The authors would also like to thank John L Harwood for NMR facility. We also acknowledge the support of Purdue University's Metabolite Profiling Facility in the acquisition and analysis of mass spectrometry data.

## Notes and references

- R. L. Siegel, K. D. Miller, H. E. Fuchs and A. Jemal, *Ca-Cancer J. Clin.*, 2021, **71**, 7–33.
- L. A. Aliperti, J. D. Predina, A. Vachani and S. Singhal, *Ann. Surg. Oncol.*, 2011, **18**, 603–607.
- C. R. Kelsey, L. B. Marks, D. Hollis, J. L. Hubbs, N. E. Ready, T. A. D'Amico and J. A. Boyd, *Cancer*, 2009, **115**, 5218–5227.
- K. Sandgren, P. Westerlinck, J. H. Jonsson, L. Blomqvist, C. T. Karlsson, T. Nyholm and P. Dirix, *Eur. Urol. Focus*, 2019, **5**, 550–560.
- G. M. Freedman and B. L. Fowble, *Oncology*, 2000, **14**, 1561–1581; discussion 1581.
- I. A. Burger, D. A. Goldman, H. A. Vargas, M. W. Kattan, C. Yu, L. Kou, V. Andikyan, D. S. Chi, H. Hricak and E. Sala, *Gynecol. Oncol.*, 2015, **138**, 554–559.
- C. R. Kelsey, K. A. Higgins, B. L. Peterson, J. P. Chino, L. B. Marks, T. A. D'Amico and J. M. Varlotto, *J. Thorac. Cardiovasc. Surg.*, 2013, **146**(768–773), e761.
- P. J. Choi, S. S. Jeong and S. S. Yoon, *Korean J. Thorac. Cardiovasc. Surg.*, 2013, **46**, 449.
- T. Nagaya, Y. A. Nakamura, P. L. Choyke and H. Kobayashi, *Front. Oncol.*, 2017, **7**, 314.
- J. Jiao, J. Zhang, F. Yang, W. Song, D. Han, W. Wen and W. Qin, *Eur. J. Pharm. Biopharm.*, 2020, **152**, 123–143.
- P. S. Low, S. Singhal and M. Srinivasarao, *Curr. Opin. Chem. Biol.*, 2018, **45**, 64–72.
- L. E. Kelderhouse, V. Chelvam, C. Wayua, S. Mahalingam, S. Poh, S. A. Kularatne and P. S. Low, *Bioconjugate Chem.*, 2013, **24**, 1075–1080.
- G. M. Van Dam, G. Themelis, L. M. Crane, N. J. Harlaar, R. G. Pleijhuis, W. Kelder, A. Sarantopoulos, J. S. De Jong, H. J. Arts and A. G. Van Der Zee, *Nat. Med.*, 2011, **17**, 1315–1319.
- I. R. Vlahov, H. K. R. Santhapuram, F. You, Y. Wang, P. J. Kleindl, S. J. Hahn, J. F. Vaughn, D. S. Reno and C. P. Leamon, *J. Org. Chem.*, 2010, **75**, 3685–3691.
- C. Wayua and P. S. Low, *J. Nucl. Med.*, 2015, **56**, 113–119.
- P.-C. Lv, J. Roy, K. S. Putt and P. S. Low, *Mol. Pharm.*, 2016, **13**, 1618–1625.
- S. M. Mahalingam, H. Chu, X. Liu, C. P. Leamon and P. S. Low, *Bioconjugate Chem.*, 2018, **29**, 3320–3331.
- A. K. Kanduluru, M. Srinivasarao and P. S. Low, *Bioconjugate Chem.*, 2016, **27**, 2157–2165.
- S. M. Mahalingam, V. Y. Dudkin, S. Goldberg, D. Klein, F. Yi, S. Singhal, K. T. O'Neil and P. S. Low, *Bioconjugate Chem.*, 2017, **28**, 2865–2873.
- J. Roy, M. Kaake and P. S. Low, *OncoTargets Ther.*, 2019, **10**, 152–160.
- S. M. Mahalingam, S. A. Kularatne, C. H. Myers, P. Gagare, M. Norshi, X. Liu, S. Singhal and P. S. Low, *J. Med. Chem.*, 2018, **61**, 9637–9646.
- M. Keramidis, V. Jossierand, C. Righini, C. Wenk, C. Faure and J. Coll, *Br. J. Surg.*, 2010, **97**, 737–743.
- M. Li, H. Li, Q. Wu, N. Niu, J. Huang, L. Zhang, Y. Li, D. Wang and B. Z. Tang, *iScience*, 2021, **24**, 102261.
- J. Zhao, G. Jin, G. Weng, J. Li, J. Zhu and J. Zhao, *Drug Discovery Today*, 2017, **22**, 1367–1374.
- H. Li, Q. Yao, W. Sun, K. Shao, Y. Lu, J. Chung, D. Kim, J. Fan, S. Long, J. Du, Y. Li, J. Wang, J. Yoon and X. Peng, *J. Am. Chem. Soc.*, 2020, **142**, 6381–6389.
- P. Garin-Chesa, L. J. Old and W. J. Rettig, *Proc. Natl. Acad. Sci. U. S. A.*, 1990, **87**, 7235–7239.
- C. Kratochwil, P. Flechsig, T. Lindner, L. Abderrahim, A. Altmann, W. Mier, S. Adeberg, H. Rathke, M. Röhrich and H. Winter, *J. Nucl. Med.*, 2019, **60**, 801–805.
- P. Busek, R. Mateu, M. Zubal, L. Kotackova and A. Sedo, *Front. Biosci.*, 2018, **23**, 1933–1968.
- E. Puré and R. Blomberg, *Oncogene*, 2018, **37**, 4343–4357.
- A. Lo, C.-P. Li, E. L. Buza, R. Blomberg, P. Govindaraju, D. Avery, J. Monslow, M. Hsiao and E. Puré, *JCI Insight*, 2017, **2**(19), e92232.
- Y. Liao, Y. Ni, R. He, W. Liu and J. Du, *J. Cancer Res. Clin. Oncol.*, 2013, **139**, 1523–1528.
- L. R. Henry, H.-O. Lee, J. S. Lee, A. Klein-Szanto, P. Watts, E. A. Ross, W.-T. Chen and J. D. Cheng, *Clin. Cancer Res.*, 2007, **13**, 1736–1741.
- T. Lindner, A. Loktev, F. Giesel, C. Kratochwil, A. Altmann and U. Haberkorn, *EJNMMI Radiopharm. Chem.*, 2019, **4**, 1–15.



- 34 E. S. Moon, F. Elvas, G. Vliegen, S. De Lombaerde, C. Vangestel, S. De Bruycker, A. Bracke, E. Eppard, L. Greifenstein, B. Klasen, V. Kramer, S. Staelens, I. De Meester, P. Van der Veken and F. Rösch, *EJNMMI Radiopharm. Chem.*, 2020, **5**, 19.
- 35 T. Lindner, A. Loktev, A. Altmann, F. Giesel, C. Kratochwil, J. Debus, D. Jäger, W. Mier and U. Haberkorn, *J. Nucl. Med.*, 2018, **59**, 1415–1422.
- 36 K. Jansen, L. Heirbaut, J. D. Cheng, J. Joossens, O. Ryabtsova, P. Cos, L. Maes, A.-M. Lambeir, I. De Meester and K. Augustyns, *ACS Med. Chem. Lett.*, 2013, **4**, 491–496.
- 37 K. Jansen, L. Heirbaut, R. Verkerk, J. D. Cheng, J. Joossens, P. Cos, L. Maes, A.-M. Lambeir, I. De Meester and K. Augustyns, *J. Med. Chem.*, 2014, **57**, 3053–3074.
- 38 Q. Miao, D. C. Yeo, C. Wiraja, J. Zhang, X. Ning, C. Xu and K. Pu, *Angew. Chem.*, 2018, **57**, 1256–1260.
- 39 X. X. Zhao, L. L. Li, Y. Zhao, H. W. An, Q. Cai, J. Y. Lang, X. X. Han, B. Peng, Y. Fei and H. Liu, *Angew. Chem.*, 2019, **131**, 15431–15438.
- 40 P. Laverman, T. van der Geest, S. Y. Terry, D. Gerrits, B. Walgreen, M. M. Helsen, T. K. Nayak, A. Freimoser-Grundschober, I. Waldhauer and R. J. Hosse, *J. Nucl. Med.*, 2015, **56**, 778–783.
- 41 S. Welt, C. R. Divgi, A. M. Scott, P. Garin-Chesa, R. D. Finn, M. Graham, E. A. Carswell, A. Cohen, S. M. Larson and L. J. Old, *J. Clin. Oncol.*, 1994, **12**, 1193–1203.
- 42 R. Rüger, F. L. Tansi, M. Rabenhold, F. Steiniger, R. E. Kontermann, A. Fahr and I. Hilger, *J. Controlled Release*, 2014, **186**, 1–10.
- 43 S. L. Slania, D. Das, A. Lisok, Y. Du, Z. Jiang, R. C. Mease, S. P. Rowe, S. Nimmagadda, X. Yang and M. G. Pomper, *J. Med. Chem.*, 2021, **64**, 4059–4070.
- 44 X. Yang, S. Nimmagadda, S. Rowe, S. Slania and M. G. Pomper, WO2019083990A2, 2019.
- 45 J. Roy, S. U. Hettiarachchi, M. Kaake, R. Mukkamala and P. S. Low, *Theranostics*, 2020, **10**, 5778.
- 46 P. S. Low, M. Srinivasarao and R. Mukkamala, WO2021055641A1, 2021.
- 47 T.-Y. Tsai, T.-K. Yeh, X. Chen, T. Hsu, Y.-C. Jao, C.-H. Huang, J.-S. Song, Y.-C. Huang, C.-H. Chien and J.-H. Chiu, *J. Med. Chem.*, 2010, **53**, 6572–6583.
- 48 J. Li, K. Chen, H. Liu, K. Cheng, M. Yang, J. Zhang, J. D. Cheng, Y. Zhang and Z. Cheng, *Bioconjugate Chem.*, 2012, **23**, 1704–1711.
- 49 J. Toms, J. Kogler, S. Maschauer, C. Daniel, C. Schmidkonz, T. Kuwert and O. Prante, *J. Nucl. Med.*, 2020, **61**, 1806–1813.
- 50 A. Loktev, T. Lindner, E.-M. Burger, A. Altmann, F. Giesel, C. Kratochwil, J. Debus, F. Marmé, D. Jäger and W. Mier, *J. Nucl. Med.*, 2019, **60**, 1421–1429.
- 51 J. Li, K. Chen, H. Liu, K. Cheng, M. Yang, J. Zhang, J. D. Cheng, Y. Zhang and Z. Cheng, *Bioconjugate Chem.*, 2012, **23**, 1704–1711.
- 52 S. L. Slania, D. Das, A. Lisok, Y. Du, Z. Jiang, R. C. Mease, S. P. Rowe, S. Nimmagadda, X. Yang and M. G. Pomper, *J. Med. Chem.*, 2021, **64**, 4059–4070.
- 53 A. Loktev, T. Lindner, E. M. Burger, A. Altmann, F. Giesel, C. Kratochwil, J. Debus, F. Marmé, D. Jäger, W. Mier and U. Haberkorn, *J. Nucl. Med.*, 2019, **60**, 1421–1429.
- 54 K. Shiga, M. Hara, T. Nagasaki, T. Sato, H. Takahashi and H. Takeyama, *Cancers*, 2015, **7**, 2443–2458.
- 55 L. Ziani, S. Chouaib and J. Thiery, *Front. Immunol.*, 2018, **9**, 414.
- 56 J. Barbazán and D. Matic Vignjevic, *Curr. Opin. Cell Biol.*, 2018, **56**, 71–79.
- 57 X. Li, S. Hu and L. Xiao, *Eur. Rev. Med. Pharmacol. Sci.*, 2015, **19**, 2112–2119.
- 58 S. Albeiroti, A. Soroosh and C. A. de la Motte, *BioMed Res. Int.*, 2015, **2015**, 790203.
- 59 F. L. Giesel, C. Kratochwil, T. Lindner, M. M. Marschalek, A. Loktev, W. Lehnert, J. Debus, D. Jäger, P. Flechsig, A. Altmann, W. Mier and U. Haberkorn, *J. Nucl. Med.*, 2019, **60**, 386–392.
- 60 S. Ballal, M. P. Yadav, E. S. Moon, V. S. Kramer, F. Roesch, S. Kumari, M. Tripathi, S. T. ArunRaj, S. Sarswat and C. Bal, *Eur. J. Nucl. Med. Mol. Imaging*, 2021, **48**, 1915–1931.
- 61 H. Chen, Y. Pang, J. Wu, L. Zhao, B. Hao, J. Wu, J. Wei, S. Wu, L. Zhao, Z. Luo, X. Lin, C. Xie, L. Sun, Q. Lin and H. Wu, *Eur. J. Nucl. Med. Mol. Imaging*, 2020, **47**, 1820–1832.
- 62 U.S. Food and Drug Administration, 2021, <https://www.fda.gov/newsevents/pressannouncements/fda-approves-new-imaging-drug-helpidentify-ovarian-cancer-lesions>.